



HAL
open science

Sensitive RHEED signature of Ti-excess enabling enhanced cationic composition control during the molecular beam epitaxy of SrTiO₃ based solid solutions

Masoumeh Razaghi Pey Ghaleh, Marc d'Esperonnat, Claude Botella, Sébastien Cueff, Romain Bachelet, Guillaume Saint-Girons

► To cite this version:

Masoumeh Razaghi Pey Ghaleh, Marc d'Esperonnat, Claude Botella, Sébastien Cueff, Romain Bachelet, et al.. Sensitive RHEED signature of Ti-excess enabling enhanced cationic composition control during the molecular beam epitaxy of SrTiO₃ based solid solutions. *CrystEngComm*, 2021, 23 (11), pp.2269-2275. 10.1039/D1CE00013F . hal-03177011

HAL Id: hal-03177011

<https://hal.science/hal-03177011>

Submitted on 22 Mar 2021

HAL is a multi-disciplinary open access archive for the deposit and dissemination of scientific research documents, whether they are published or not. The documents may come from teaching and research institutions in France or abroad, or from public or private research centers.

L'archive ouverte pluridisciplinaire **HAL**, est destinée au dépôt et à la diffusion de documents scientifiques de niveau recherche, publiés ou non, émanant des établissements d'enseignement et de recherche français ou étrangers, des laboratoires publics ou privés.

Sensitive RHEED signature of Ti-excess enabling enhanced cationic composition control during the molecular beam epitaxy of SrTiO₃ based solid solutions

Masoumeh Razaghi, Marc d'Esperonnat, Claude Botella, Sébastien Cueff, Romain Bachelet and Guillaume Saint-Girons

Institut des Nanotechnologies de Lyon, INL-CNRS/UMR5270, Ecole Centrale de Lyon, 36 avenue Guy de Collongue 69134 Ecully, France

ABSTRACT

Molecular beam epitaxy (MBE) is the best suited technique to engineer perovskite oxide properties, thanks to individual atom evaporation from elemental sources. Unfortunately, significant source drift often prevents exploiting this advantage, and improving the control of the composition of MBE grown oxide thin layers remains a challenge. In this context, in-situ reflection high energy electron diffraction (RHEED) has been for long identified as a useful tool, as surface reconstructions and RHEED oscillations depend on oxide cationic composition. We show here that monitoring the appearance of half-order streaks along the [210] RHEED azimuths of Ti-rich surfaces provides enhanced control of the cationic composition of SrTiO₃ thin layers as compared to the more common strategy relying on [100] azimuths monitoring. We also provide quantitative evaluation of the uncertainty on composition control enabled by this method, namely +/- 6.7%. In the end, we describe an original procedure to control the composition of perovskite oxide quaternary solid solutions.

I. INTRODUCTION

Functional oxides with perovskite structure (general formula ABO_3) present a wide range of physical properties (conductivity, ferromagnetism, ferroelectricity, piezoelectricity, thermoelectricity,...) attractive in various domains.¹ These properties depend on composition, and in particular on the ratio $[A]/[B]$ between the cation concentrations,^{2,3} which must be accurately controlled. $SrTiO_3$ (STO), archetypal perovskite oxide, is used in non-volatile memories, smart sensors, energy harvesters,... Bulk stoichiometric STO ($[A]/[B] = 1$) is a band insulator. It becomes ferroelectric with tunable Curie temperature when submitted to partial isovalent cationic substitution of Ba on A site.⁴ Partial aliovalent substitution (typically of La on A site or Nb on B site)^{5,6} or introduction of oxygen vacancies⁷ in STO induces tunable electrical conductivity (with high carrier mobility) and remarkable thermoelectric properties. When subjected to cationic stoichiometry deviation ($[A]/[B] \neq 1$), STO shows resistive switching behavior,⁸ enhanced charge carrier mobility,⁹ as well as tunable electrical and thermal conductivity.^{10,11}

Molecular beam epitaxy (MBE) is particularly well suited to control perovskite oxide composition and physical properties thanks to elemental sources.¹² However, such control remains to date a challenge due to source drift. The latter causes poor growth reproducibility, which makes inoperable calibration strategies using post-growth (ex-situ) composition measurements (based, for instance, on X-ray diffraction (XRD)). Monitoring Reflection High Energy Electron Diffraction (RHEED) oscillations enables in-situ STO composition control with an accuracy in the 1% range.¹³ However, this procedure is not strictly speaking real-time as it requires employing SrO/TiO₂ monolayers (ML) alternated growth and observing oscillations during a large number of alternations, which is not compatible with the growth of any structure. Consequently, as ex-situ calibrations although to a lesser extent, its efficiency is limited by source drift. Solving the source drift issue requires a truly real-time procedure, which is the case of STO(001) surface reconstructions monitoring using in-situ RHEED.^{14,15,16} This method, the accuracy of which has to date not been reported, relies on the dependence of these reconstructions on the Sr/Ti surface coverage.^{17,18,19,20,21} It is operated by monitoring the appearance of half-order streaks along the [100] (respectively [110]) RHEED azimuth, signature Ti-rich (respectively Sr-rich) surfaces, and by tuning the elemental growth rates to prevent their formation,^{14,15} or to maintain a TiO₂-saturated STO surface in the case of metalorganic assisted oxide MBE¹⁶ where titanium tetraisopropoxide (TTIP) used as Ti source enables self-limited Ti incorporation.^{22,23}

In this context, we show here that the observation of half-order streaks along both [100] and [210] azimuths associated with the Ti-rich STO surface reconstruction is preceded by that of half-order streaks along the [210] azimuth only, and that using this signature enables significant accuracy

improvement for in-situ real-time STO composition control. We quantify this accuracy, and compare it to that provided by high resolution X-ray diffraction measurements (XRD). In the end, we propose a strategy to control the cationic composition of quaternary (La,Sr)TiO₃ solid solutions using RHEED reconstructions.

II. EXPERIMENTAL

The samples considered in the following were grown by solid source MBE on (001)-oriented STO substrates under a molecular oxygen partial pressure of 5×10^{-7} Torr at 700°C, as detailed in the supplementary material.

In a first experiment, one SrO ML was deposited on a clean, TiO₂-terminated STO substrate treated using a HF-based buffered oxide etchant (BOE),²⁴ followed by one TiO₂ ML to recover the initial complete TiO₂ termination. During this process, the RHEED pattern along the [110] azimuth was continuously recorded. The complete operation was reproduced twice in order to record the evolution of the RHEED patterns along the [100] and [210] azimuths.

In a second experiment, a series of ~30 nm thick STO epitaxial layers with various cationic compositions was grown. X-ray photoemission spectroscopy (XPS) was used to estimate the [Sr]/[Ti] atomic concentrations ratio, with a relative uncertainty in the $\pm 2\text{-}3\%$ range.²⁵ XRD (respectively X-ray reflectivity (XRR)) was used to measure the out-of-plane lattice parameter *c* (respectively the thickness) of these layers.

In the end, in a third experiment, three La_{*x*}Sr_{1-*x*}TiO₃ (LSTO) / STO heterostructures with *x* ~ 0.2 and [A]/[B] = ([La]+[Sr])/Ti ~ 1 were grown. Spectroscopic ellipsometry was used to evaluate the charge carrier concentration and hence the La substitution ratio *x*.

III. RESULTS AND DISCUSSION

As mentioned earlier, STO surface reconstructions depend on Sr/Ti surface coverage in usual MBE conditions. 50% SrO/50% TiO₂ STO(001) surfaces are reconstruction-free,¹⁴ Ti-rich surfaces present two-domain (2x1), c(6x2), c(4x4) or c(4x2) reconstructions depending on oxygen partial pressure,^{17,18,19,26} and Sr-rich surfaces present a $\sqrt{2} \times \sqrt{2}$ R45° reconstruction.²¹ The results of the first experiment (alternated SrO/TiO₂ deposition), summarized in Fig.1, are consistent with this well documented behavior.

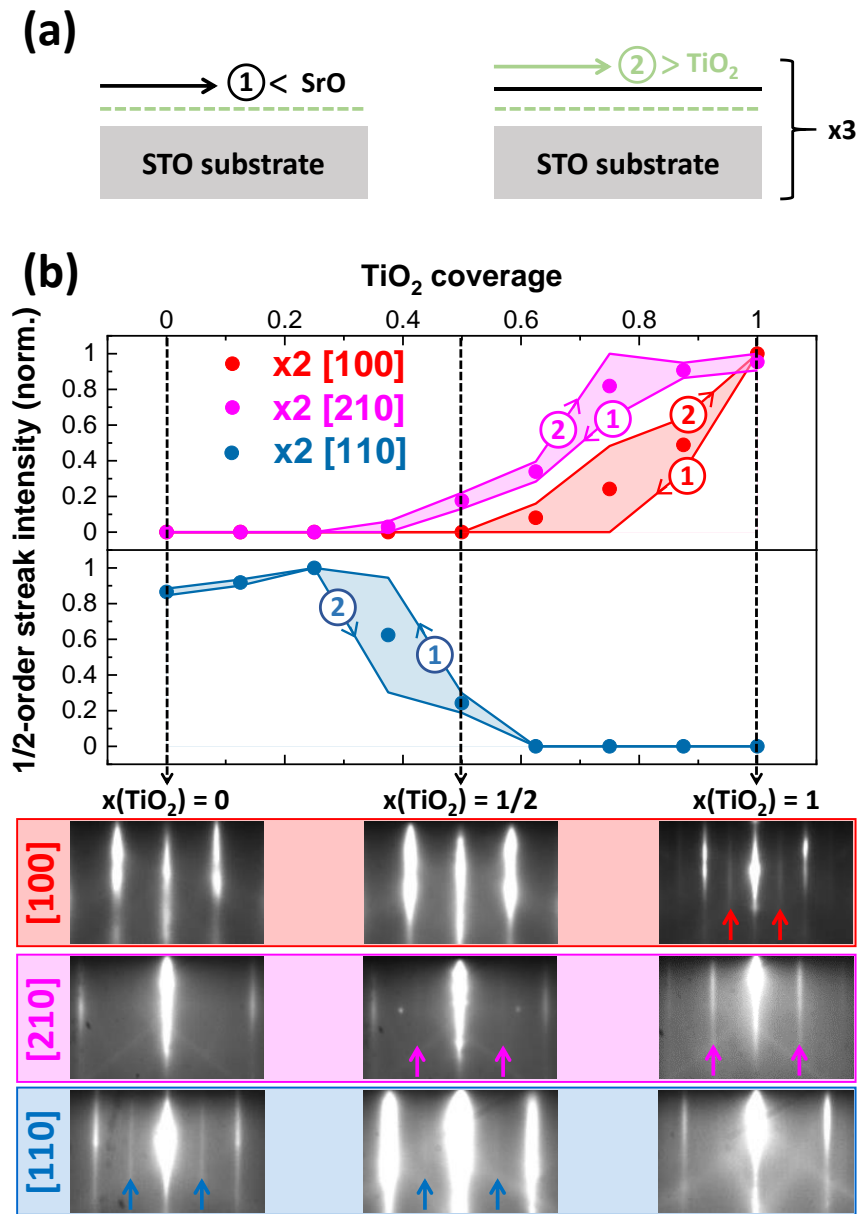


Fig.1 : (a) Growth sequence used during the first experiment. On a TiO₂ terminated STO(001) substrate (----- = initial complete TiO₂ termination), a SrO ML is deposited (————→ ①<) until complete SrO coverage is reached (————) while monitoring the evolution of the RHEED pattern along one azimuth. Then, a TiO₂ ML is deposited (————→ ②>), keeping on with RHEED monitoring along the same azimuth. This procedure is carried out three times to record the RHEED pattern evolution along the [110], [100] and [210] azimuths. (b) Evolution of the intensity of the half-order streaks along the [100], [210] and [110] azimuths during SrO deposition (arrowheads labelled 1 on curves) and TiO₂ deposition (arrowheads labelled 2 on curves) as a function of the TiO₂ coverage $x(\text{TiO}_2)$ (the SrO coverage $x(\text{SrO})$ obeys $x(\text{SrO})=1- x(\text{TiO}_2)$). Bottom panel: RHEED patterns recorded at different TiO₂ coverages. Arrows highlight the half-order streaks.

The RHEED pattern evolves with surface coverage from half-order streaks along the [110] azimuth for a complete SrO coverage ($x(\text{TiO}_2) = 0$ ($\sqrt{2} \times \sqrt{2}$ $R45^\circ$ -reconstructed Sr-rich surface)²¹ to half-order streaks along both [100] and [210] azimuths for a complete TiO_2 coverage ($x(\text{TiO}_2) = 1$, (2x1)-reconstructed Ti-rich surface^{17,27}). Notwithstanding a slight hysteresis, this evolution does not strongly depend on whether SrO or TiO_2 is the topmost (growing) atomic layer.

On the Sr-rich side, the intensity of the half-order streaks along the [110] azimuth becomes maximal for a SrO coverage of ~ 0.75 ML ($x(\text{TiO}_2) \sim 0.25$), consistent with Ref.21 stipulating that the $\sqrt{2} \times \sqrt{2}$ $R45^\circ$ reconstruction is a partially SrO-deficient SrO-terminated surface. On the Ti-rich side, the intensity of the half-order streaks along the [100] azimuth is maximal for $x(\text{TiO}_2) = 1$, as expected from some models of the two-domain (2x1)-reconstructed Ti-rich surface involving periodic arrangement of O vacancies in a complete TiO_2 surface atomic plane.^{17,28}

Interestingly, the half-order streaks along the [210] azimuth, sometimes associated with another signature of the two-domain (2x1)-reconstruction,¹⁴ appear at lower TiO_2 coverage than the half-order streaks along the [100] azimuth and their intensity is maximum at lower TiO_2 coverage too (namely $x(\text{TiO}_2) \sim 0.8$). One may speculate that atomic ordering at the origin of the (2x1) reconstruction is anisotropic, starting earlier along $\langle 210 \rangle$ surface axes, or that the formation of the (2x1) reconstruction is preceded by another surface atomic arrangement leading to half-order streaks along the [210] azimuths only. Either way, this shows that half-order streaks along the [210] azimuths are an earlier signature of Ti-excess on the STO surface than half-order streaks along the [100] azimuths, conventionally used as marker to monitor STO composition during growth.¹⁴

Lastly, for $x(\text{TiO}_2) = 1/2$, half-order streaks are detected along both [210] and [110] azimuths, suggesting the coexistence of reconstructed SrO-terminated and TiO_2 -terminated domains in equal proportion. Noticeably, in codeposition conditions (Sr and Ti deposited simultaneously), half-order streaks are absent from the RHEED patterns over a significant composition range around $x(\text{TiO}_2) = 1/2$, probably due to larger surface disorder and larger growth rate.

We now show that tracking the half-order streaks along the [210] azimuth enables improved STO composition control. The out-of-plane lattice parameters of the STO layers of the second experiment (measured by XRD) are shown as a function of their cationic composition (measured by XPS and indexed by δ in $\text{Sr}_{1+\delta}\text{TiO}_3$) in Fig.2, along with the RHEED patterns observed at the end of the growth.

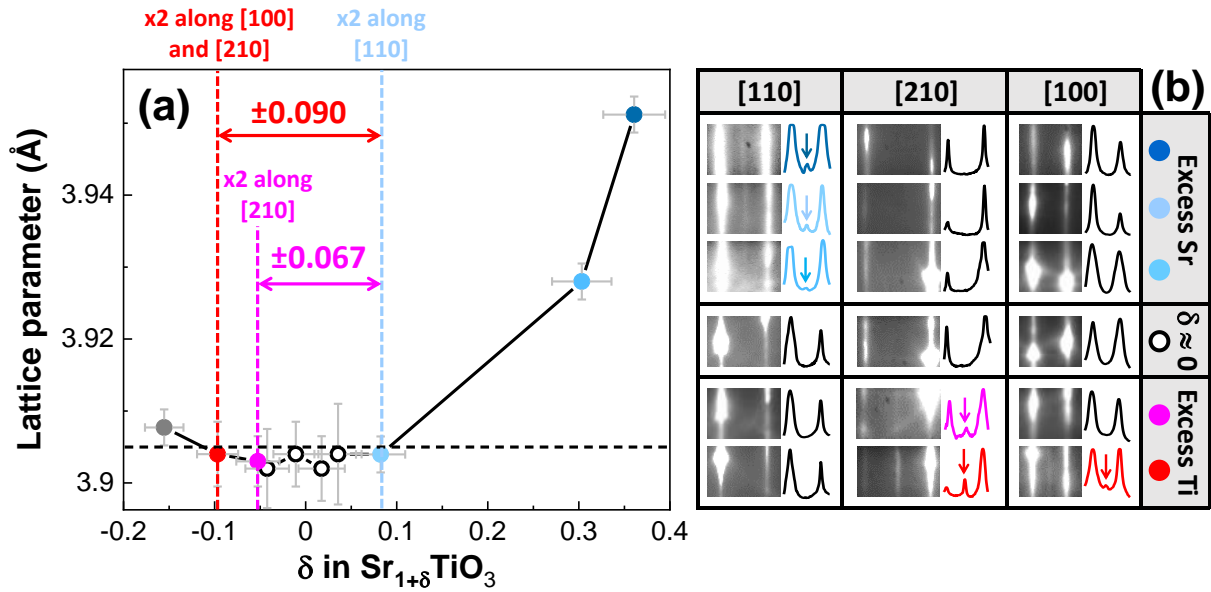


Fig.2 : (a) Out-of-plane lattice parameter of the STO layers as a function of their cationic composition indexed by δ in $Sr_{1+\delta}TiO_3$. The dot color code corresponds to the surface reconstruction observed at the end of the growth : ●, ●, ● = x2 along the [110] azimuth, ○ = no reconstruction ($\delta \approx 0$), ● = x2 along [210] only, ● = x2 along both [210] and [100], and ● = no reconstruction on the very Ti-rich surface due to surface disorder. ----- indicate the value of bulk STO lattice parameter (3.905 Å). Zooms on the corresponding RHEED patterns (selected region is shown in the supplementary material) are displayed in (b), along with intensity profiles. Arrows highlight the half-order streaks.

As expected, the STO lattice parameter is minimal and close to the bulk value when δ is near 0, and increases for larger $|\delta|$ values as defects due to deviation from stoichiometric composition cause lattice unit-cell inflation.^{29,11,30,26} The composition range over which the lattice parameter remains constant and minimal is quite large, corresponding to $\delta = \pm 9\%$. Deviation from stoichiometric composition goes hand in hand with the observation of the RHEED patterns commented above, as excess cations segregate toward the surface or accumulate at the growth front. On the Sr-rich side, half-order streaks along the [110] azimuth are detected when δ exceeds 0.08, while on the Ti-rich side, half-order streaks along both [100] and [210] azimuths are detected when δ gets smaller than -0.09. Besides, for $\delta = -0.16$, surface reconstructions are no longer observed due to increased surface disorder and roughness caused by Ti excess. The strategy of STO composition control based on monitoring the half-order streaks along the [110] and [100] azimuths^{14,15} thus provides an uncertainty of about $\pm 9\%$ on δ estimation, comparable to that provided by ex-situ XRD measurements. As for sub-ML TiO_2 and SrO alternated growth, half-order streaks along the [210] azimuths provide an earlier signature of Ti excess on the surface than half-order streaks along the [100] azimuths, and allow detecting smaller Ti excesses in the layers, corresponding to $\delta < -0.05$. This shows that monitoring the appearance of half-order

streaks along the [110] and [210] azimuths (instead of [110] and [100]) significantly improves the accuracy on STO composition control, reducing the uncertainty on δ down to $\pm 6.7\%$, which is also better than that provided by XRD measurements. Such improvement is particularly valuable in the context detailed in the introduction where STO properties are strongly affected by deviations from the stoichiometric [Sr]/[Ti] ratio.

As mentioned in the introduction, partially substituting divalent Sr by trivalent La in SrTiO_3 to form $(\text{La}_x\text{Sr}_{1-x})\text{TiO}_3$ (LSTO) allows obtaining N-type thin layers, the electrical conductivity and thermoelectric properties of which can be tuned by varying the La concentration.^{31,32,33,34} We present in the following a method to control in-situ the composition of such LSTO thin layers using RHEED reconstructions.

The three LSTO/STO heterostructures considered for these purpose were grown as follows (third experiment): the 10 nm thick STO layer was grown at constant Sr beam equivalent pressure $F_0(\text{Sr})$ measured before growth using a Bayard-Alpert gauge. During STO growth, the Ti cell temperature was tuned to prevent the appearance of half-order streaks along the [110] and [210] azimuths of the RHEED pattern, so that the resulting STO layer has stoichiometric composition within $\pm 6.7\%$ uncertainty. Practically speaking, this was done by repeating the following sequence:

- (i) constant monitoring of the [110] and [210] RHEED azimuths during Sr and Ti codeposition
- (ii) closing of the Sr (respectively Ti) shutter each time half-order streaks are observed along the [110] (respectively [210]) azimuth until their complete disappearance (to compensate the surface cationic excess)
- (iii) growth stop and increase (respectively decrease) of the Ti cell temperature to approach stoichiometric growth conditions
- (iv) growth re-start

until half order streaks are no longer observed along any azimuth.

Then, for the growth of the LSTO layers with a targeted La atomic composition of 20% ($(\text{La}_{0.2}\text{Sr}_{0.8})\text{TiO}_3$), the Ti cell temperature was kept constant to the value leading to stoichiometric STO growth, and the Sr cell temperature was reduced so that the Sr beam equivalent pressure is $0.8x F_0(\text{Sr})$. LSTO growth was then started by co-depositing La, Sr and Ti, and the La cell temperature was adjusted to obtain three different RHEED patterns for each of the three samples, namely half-order streaks along the [110] azimuth for one sample, no surface reconstruction for the second sample, and half-order streaks along both [100] and [210] azimuths, using the 4-step procedure described above.

Fig.3 shows the RHEED patterns (recorded at the end of the growth) and the XRD radial scans measured on these heterostructures.

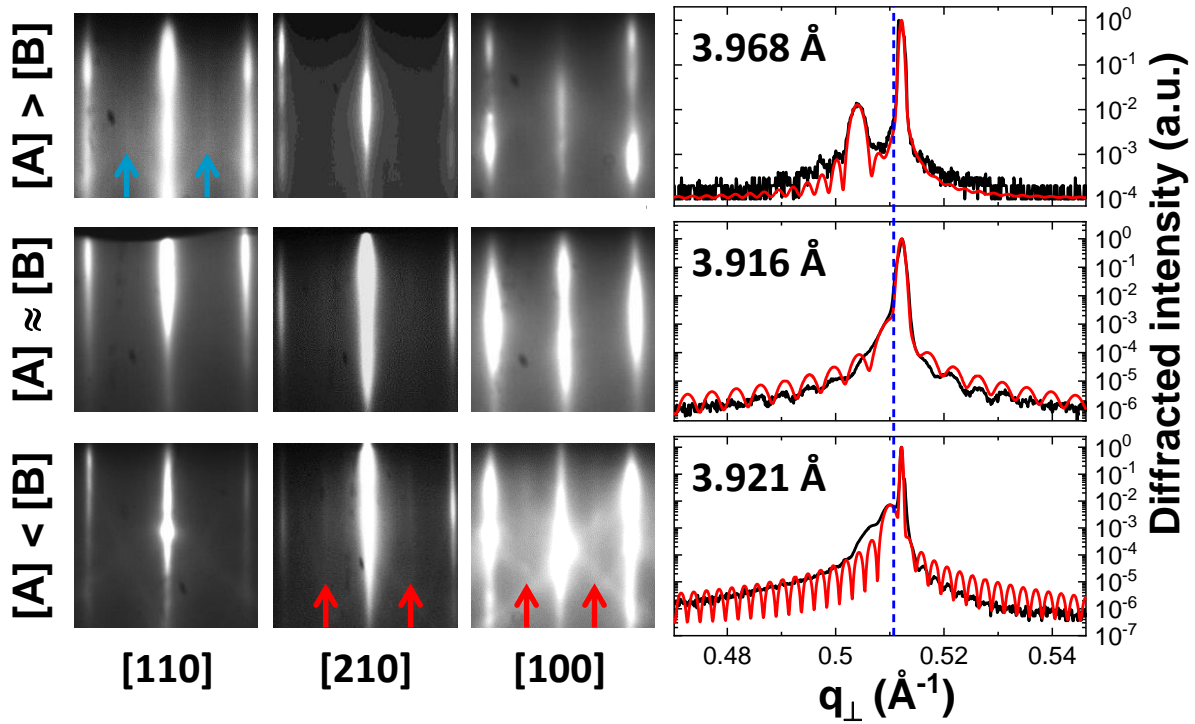


Fig.3 :RHEED patterns (at the end of the growth, half-order streaks highlighted by arrows) and XRD radial scans recorded on LSTO/STO heterostructures with various compositions (— = experimental curves, — = fit). [A] (respectively [B]) designates the total A site (respectively B site) composition in ABO_3 . q_{\perp} stands for the out-of-plane diffraction vector. ----- indicate the position of the maximum of the nearly-stoichiometric LSTO diffraction peak (corresponding to a lattice parameter of 3.916 Å).

For the sample presenting a reconstruction-free RHEED pattern at the end of LSTO growth ($[A] \approx [B]$ in Fig.3), the LSTO lattice parameter (3.916 Å) is minimal. For the sample presenting half-order streaks along the [110] RHEED azimuth ($[A] > [B]$ in Fig.3), as for that presenting half-order streaks along both [210] and [100] azimuths ($[A] < [B]$ in Fig.3), the lattice parameter is increased, to 3.968 Å and 3.921 Å, respectively. This shows that LSTO behaves as STO with respect to cationic composition in terms of lattice parameter inflation and surface reconstructions, and that therefore the latter can be used to monitor composition in-situ using RHEED. It has to be noted here that as in the case of STO, half-order streaks appear at lower surface Ti excess along the [210] azimuth than along the [100] azimuth (not shown).

We now discuss the properties of the LSTO/STO heterostructure grown in near stoichiometric conditions ($[A] \approx [B]$ in Fig.3), depicted in Fig.4(a).

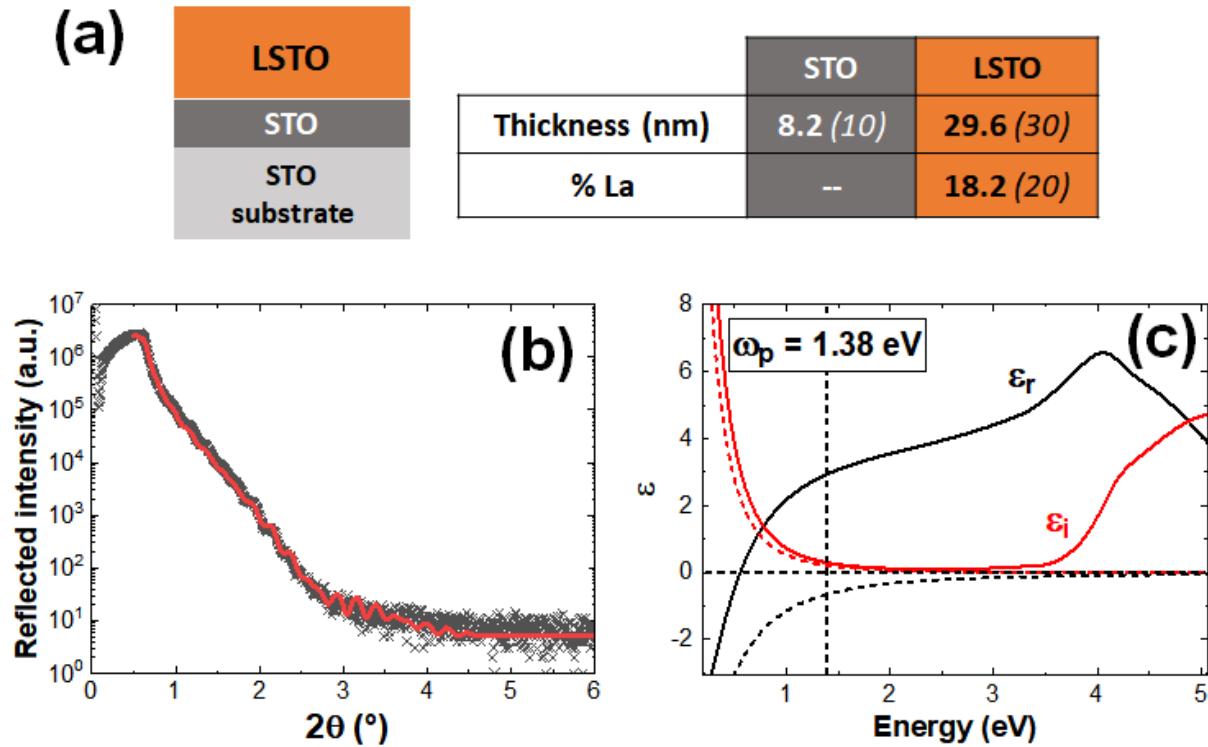


Fig.4 : (a) Schematic of the LSTO/STO structure grown in near stoichiometric conditions, and associated thicknesses and La composition respectively deduced from XRR and spectrometric ellipsometry measurements. In the table, measured values are bolded and nominal (targeted) values are bracketed. (b) XRR spectrum recorded on the sample (—) and associated fit (—). (c) Real (ϵ_r , —) and imaginary (ϵ_i , —) parts of the permittivity of the STO layer measured by spectroscopic ellipsometry. The free charge carrier contribution in the low energy range can be described by a Drude contribution (---, - - -).

The XRD radial scan displayed in Fig.3 attests for the excellent structural quality of the LSTO layer, with an excellent fit between the experimental data and the model calculated for an ideal structure, free of any defect. The lattice parameter of the LSTO layer, namely $3.916 \pm 10^{-3} \text{ \AA}$, is slightly larger than the $3.907\text{-}3.908 \text{ \AA}$ expected from theoretical calculations for bulk $(\text{La}_{0.2}\text{Sr}_{0.8})\text{TiO}_3$,^{35,36} but is among the lowest reported experimental values,^{37,38,39,40} suggesting successful control of the layer composition and a low concentration of defects prone to inflate the unit cell volume. The thicknesses of the STO and LSTO layers estimated from XRR are reasonably close from the targeted values (table in Fig.4), which is another indication of the reliability of the method. The permittivity of the LSTO layer was measured using spectroscopic ellipsometry (Fig.4(c)). It presents a free charge carrier contribution with an increase of the imaginary part ϵ_i and a decrease of its real part ϵ_r below $\sim 1.5 \text{ eV}$. This behavior is usually described by a Drude function ϵ_D ⁴¹ reading:

$$\varepsilon_D(\omega) = -\frac{\omega_p^2}{-\omega^2 + i \cdot \Gamma_D \omega}, \quad \text{Eq.1}$$

where ω is the frequency, Γ_D a broadening term and ω_p the plasma frequency, related to the free charge carrier concentration N by :

$$\omega_p = \sqrt{\frac{N \cdot e^2}{\varepsilon_0 \cdot m^*}} \quad \text{Eq.2}$$

where e is the electron charge, ε_0 the vacuum permittivity and m^* the charge carrier effective mass. Excellent fit of the ellipsometry data was obtained with $\omega_p = 1.38$ eV (2.094×10^{15} rad.s⁻¹, see supplementary material). The free electron mass in LSTO is about $2.2 \times m_0$,^{42,57} where $m_0 = 9.11 \times 10^{-31}$ kg is the electronic mass, leading to a free electron concentration N of about 3.03×10^{21} cm⁻³ (Eq.2). As every La atom delivers one free electron to the structure,⁵¹ this corresponds to a La atomic concentration of about 18.2%, for a unit-cell volume of 59.71 \AA^3 ($= 3.905^2 \times 3.916 \text{ \AA}^3$). This La atomic concentration is very close to the targeted 20% value, further confirming the efficiency of our optimized RHEED based procedure to control the composition of complex perovskite oxide solid solutions.

IV. CONCLUSION

The study reported here shows that half-order streaks along the [210] RHEED azimuths are an earlier signature of Ti-excess on the STO surface than half-order streaks along the [100] azimuths, and that this can be leveraged to improve the accuracy in controlling STO composition in-situ and in real-time using RHEED monitoring. This work also estimates the corresponding uncertainty on composition control, namely +/- 6.7% using the [210] azimuth, to be compared to +/- 9% using the [100] azimuth. Moreover, we describe a procedure to control the composition of perovskite oxide quaternary solid solutions. These results pave the way towards an improved control of the properties of SrTiO₃ based solid solutions, which strongly depend on their composition. Furthermore, the method can be operated in-situ and in real-time during growth, enabling dynamic correction of elemental cell drift. It does not impose constraints on the growth conditions, and in particular it does not require using layer-by-layer growth, in contrast to RHEED oscillation based methods.¹³ Besides, accuracy on composition control can be improved by reducing the growth rate, which should reduce surface roughness and thus allow detecting half-order streaks at lower Sr or Ti excesses. The method can also be automated, using feedback loops to control effusion cell temperatures from half-order streak intensities. In the end, the method can be applied to any perovskite oxide for which composition-dependent surface

reconstructions are observed, which is at least the case for STO, for $(\text{La}_x\text{Sr}_{1-x})\text{TiO}_3$ solid solutions as shown here, for ferroelectric $(\text{Ba}_x\text{Sr}_{1-x})\text{TiO}_3$ alloys⁴³ and probably many others.

SUPPLEMENTARY MATERIAL

See the supplementary material for the complete RHEED data, the method used to estimate the thin layer composition using XPS, the complete X-ray diffraction data, the detailed procedure used for STO and LSTO growth, and full details on ellipsometry measurements.

ACKNOWLEDGMENTS

The authors gratefully thank Philippe Regreny and Jean-Baptiste Goure for their technical support. This work benefited from the support of the projects LILIT ANR-16-CE24-0022, MITO ANR-17-CE05-0018 and DIAMWAFEL ANR-15-CE08-0034.

REFERENCES

- 1 L.J. Tejuca, and J.L.G. Fierro, "Properties and Applications of Perovskite Type Oxides", Eds Marcel Dekker, New York (1993).
- 2 C.N.R. Rao, J. Gopalakrishnan and K. Vidyasagar, Indian J. Chem. Sect. A **23A**, 265 (1984).
- 3 D.M. Smyth, Annu. Rev. Mater. Sci. **15**, 329 (1985).
- 4 A.D. Hilton, and B.W. Ricketts, J. Phys. D: Appl. Phys. **29**, 1321 (1996).
- 5 T. Okuda, K. Nakanishi, S. Miyasaka, and Y. Tokura, Phys. Rev. B **63**, 113104 (2001).
- 6 J. Son, P. Moetakef, B. Jalan, O. Bierwagen, N.J. Wright, R. Engel-Herbert, and S. Stemmer, Nature Materials **9**, 482 (2010).
- 7 H.N. Lee, S.S.A. Seo, W.S. Choi, and C.M. Rouleau, Scientific Reports **6**, 19941 (2016).
- 8 E. Mikheev, J. Hwang, A.P. Kajdos, A.J. Hauser, and S. Stemmer, Scientific Reports **5**, 11079 (2015).
- 9 S. Kobayashi, Y. Mizumukai, T. Ohnishi, N. Shibata, Y. Ikuhara, and T. Yamamoto, ACS Nano **9**, 10769 (2015).
- 10 T. Ohnishi, K. Shibuya, T. Yamamoto, and M. Lippmaa, J. Appl. Phys. **103**, 103703 (2008).
- 11 C.M. Brooks, R.B. Wilson, A. Schäfer, J.A. Mundy, M.E. Holtz, D.A. Muller, J. Schubert, D.G. Cahill, and D.G. Schlom, Appl. Phys. Lett. **107**, 051902 (2015).

- 12 D.G. Schlom, L.Q. Chen, X. Pan, A. Schmehl, and M.A. Zurbuchen, *J. Am. Ceram. Soc.* **91**, 2429, (2008).
- 13 J.H. Haeni, C.D. Theis, and D.G. Schlom, *Journal of Electroceramics* **4**, 385, (2000).
- 14 Z. Yu, Y. Liang, C. Overgaard, X. Hu, J. Curless, H. Li, Y. Wei, B. Craigo, D. Jordan, R. Droopad, J. Finder, K. Eisenbeiser, D. Marshall, K. Moore, J. Kulik, and P. Fejes, *Thin Solid Films* **462**, 51, (2004).
- 15 P. Fisher, H. Du, M. Skowronski, P.A. Salvador, O. Maksimov, and X. Weng, *J. Appl. Phys.* **103**, 013519, (2008).
- 16 A.P. Kajdos, and S. Stemmer, *Appl. Phys. Lett.* **105**, 191901, (2014).
- 17 M.R. Castell, *Surf Sci* **505**, 1 (2002).
- 18 N. Erdman, K.R. Poeppelmeier, M. Asta, O. Warschkow, D.E. Ellis, and L.D. Marks, *Nature* **419**, 56, (2002).
- 19 O. Warschkow, M. Asta, N. Erdman, K.R. Poeppelmeier, D.E. Ellis, L.D. Marks, *Surf Sci* **573**, 446 (2004).
- 20 Q.D. Jiang, and J. Zegenhagen, *Surf. Sci.* **425**, 343 (1999).
- 21 S. Ogawa, K. Kato, N. Nagatsuka, S. Ogura, and K. Fukutani, *Phys. Rev. B* **96**, 085303 (2017).
- 22 B. Jalan, R. Engel-Herbert, N.J. Wright, and S. Stemmer, *J. Vac. Sci. Technol. A* **27**, 461 (2009).
- 23 B. Jalan, P. Moetakef, and S. Stemmer, *Appl. Phys. Lett.* **95**, 032906 (2009).
- 24 G. Koster, B.L. Kropman, G.J.H.M. Rijnders, D.H.A. Blank, and H. Rogalla, *Appl. Phys. Lett.* **73**, 2920, (1998).
- 25 R. Hesse, T. Chassé, P. Streubel and R. Szargan, *Surf. Interf. Anal.* **36**, 1373, (2004).
- 26 Q.D. Jiang, and J. Zegenhagen, *Surf. Sci.* **425**, 343 (1999).
- 27 N. Erdman, O. Warschkow, M. Asta, K. R. Poeppelmeier, D. E. Ellis, and L. D. Marks, *J. Am. Chem. Soc.* **125**, 10050 (2003).
- 28 N. Erdman, O. Warschkow, M. Asta, K. R. Poeppelmeier, D. E. Ellis, and L. D. Marks, *J. Am. Chem. Soc.* **125**, 10050 (2003).
- 29 C.M. Brooks, L. Fitting Kourkoutis, T. Heeg, J. Schubert, D. A. Muller, and D. G. Schlom, *Appl. Phys. Lett.* **94**, 162905 (2009).
- 30 T. Ohnishi, K. Shibuya, T. Yamamoto, and M. Lippmaa, *J. Appl. Phys.* **103**, 103703 (2008).
- 31 T. Okuda, K. Nakanishi, S. Miyasaka, and Y. Tokura, *Phys. Rev. B* **63**, 113104 (2001).
- 32 B. Jalan, and S. Stemmer, *Appl Phys Lett.* **97**, 42106 (2010).
- 33 J. Son, P. Moetakef, B. Jalan, O. Bierwagen, N.J. Wright, R. Engel-Herbert, and S. Stemmer, *Nature Materials* **9**, 482 (2010).
- 34 J. Ravichandran, W. Siemons, H. Heijmerikx, M. Huijben, A. Majumdar, and R. Ramesh, *Chem Mater.* **22**, 3983 (2010).
- 35 R. Moos, and K.H. Härdtl, *J. Am. Ceram. Soc.* **80**, 2549 (1997).

- 36 A. Janotti, B. Jalan, S. Stemmer, and C.G. Van de Walle, *Appl. Phys. Lett.* **100**, 262104 (2012).
- 37 J. Ravichandran, W. Siemons, M. L. Scullin, S. Mukerjee, M. Huijben, J. E. Moore, A. Majumdar, and R. Ramesh, *Phys. Rev. B* **83**, 035101 (2011).
- 38 W.S. Choi, H.K. Yoo, and H. Ohta, *Adv. Funct. Mater.* **25**, 799 (2015).
- 39 M. Choi, A.B. Posadas, C.A. Rodriguez, A. O'Hara, H. Seinige, A.J. Kellock, M.M. Frank, M. Tsoi, S. Zollner, V. Narayanan, and A.A. Demkov, *J. Appl. Phys.* **116**, 043705 (2014).
- 40 M. Apreutesei, R. Debord, M. Bouras, P. Regreny, C. Botella, A. Benamrouche, A. Carretero-Genevri, J. Gazquez, G. Grenet, S. Pailhès, G. Saint-Girons, and R. Bachelet, *Sci. Technol. Adv. Mater.* **18**, 435 (2017).
- 41 W.L. Bade, *J. Chem. Phys.* **27**, 1280 (1957).
- 42 M. Bouras, D. Han, S. Cueff, R. Bachelet, and G. Saint-Girons, *ACS Photonics* **6**, 1755 (2019).
- 43 Y. Yoneda, K. Sakaue and H. Terauchi, *Surf. Sci.* **529**, 283 (2003).